A mechanistic account of value computation in the human brain

Marios G. Philiastides[a,b,1], Guido Biele[a,b], and Hauke R. Heekeren[a,b,c]

[a]Max Planck Institute for Human Development, 14195 Berlin, Germany; [b]Max Planck Institute for Human Cognitive and Brain Sciences, 04303 Leipzig, Germany; and [c]Department of Education and Psychology, Freie Universität Berlin, 14195 Berlin, Germany

Edited* by Leslie G. Ungerleider, National Institute of Mental Health, Bethesda, MD, and approved April 13, 2010 (received for review February 11, 2010)

To make decisions based on the value of different options, we often have to combine different sources of probabilistic evidence. For example, when shopping for strawberries on a fruit stand, one uses their color and size to infer—with some uncertainty—which strawberries taste best. Despite much progress in understanding the neural underpinnings of value-based decision making in humans, it remains unclear how the brain represents different sources of probabilistic evidence and how they are used to compute value signals needed to drive the decision. Here, we use a visual probabilistic categorization task to show that regions in ventral temporal cortex encode probabilistic evidence for different decision alternatives, while ventromedial prefrontal cortex integrates information from these regions into a value signal using a difference-based comparator operation.

decision making | probabilistic evidence | value | difference comparator | functional MRI

In our everyday lives we often have to combine different sources of probabilistic information to make decisions that are more likely to produce desirable outcomes. For instance, imagine choosing strawberries on a fruit stand on the basis of their size and color, trying to increase the likelihood your strawberry smoothie will taste delicious. Despite much progress in understanding the neural systems that mediate reward- and value-based decision making in humans (1–8), including recent reports of value-based modulations in sensory cortex (9–11), it remains unclear how the brain represents different sources of probabilistic information and how they are used to compute the value signal necessary to make a decision.

Research on perceptual decision making has already established that category-selective regions in sensory cortex encode the amount of perceptual information (i.e., *sensory* evidence) used in the decision process (12–17). To date it remains unclear, however, whether sensory regions also represent the amount of probabilistic reward information (i.e., *probabilistic* evidence) associated with different decision alternatives during value-based decisions. The lack of empirical affirmation that such regions exist has made it difficult to provide a mechanistic account of how different sources of probabilistic evidence are combined to compute value. Despite the fact that several studies on value-based decision making have consistently implicated the medial prefrontal cortex in encoding expected value signals (18–27), it remains unknown whether it is directly involved in computing the value signal needed to make the decision (by combining different sources of probabilistic evidence) or whether it merely reflects the consequence of the decision process.

Notably, the only available empirical evidence that could provide mechanistic insights into the computation of choice values comes from work on perceptual decision making. Specifically, this line of research has shown that, for binary perceptual choices, decision variables are computed by integrating the difference of the outputs of neural populations, tuned to sensory evidence for each decision alternative (12–17, 28). It is currently unknown whether this mechanism also applies to the neural implementation of value-based decision making.

To investigate whether a similar mechanism might be at work during value-based decision making based on probabilistic information, we formed two hypotheses. First, we hypothesized that distinct brain regions represent probabilistic evidence for the different decision alternatives during value-based decision making. Second, we hypothesized that, similar to perceptual decision making, signals from these regions are combined, using a difference-based comparator operation, to compute decision value signals.

Results

To test the above hypotheses, we collected functional MRI (fMRI) data while subjects performed a binary probabilistic categorization task (Fig. 1*A*). In each trial participants viewed four images of faces and houses, presented simultaneously on the screen, and had to decide whether a face (F) or a house (H) choice would be rewarded. Importantly, to ensure equal amounts of face and house sensory evidence on each trial, 2 faces and 2 houses, pooled randomly with replacement from a set of 10 images (5 faces and 5 houses), were presented together.

We manipulated expected value by manipulating reward probability (29). Specifically, reward probability was based on probabilistic information associated with each image as determined by a set of preassigned image weights (Fig. 1*B*). Subjects had to combine the amount of probabilistic evidence given by the presented face and house images to compute the value signal required to make the choice that was more likely to lead to a reward. Reward on a trial was delivered probabilistically according to the sum of weights assigned to the presented images (*Materials and Methods*).

The weights for the 10 images were balanced between faces and houses (faces: positive weights; houses: negative weights) so that face and house choices had, on average, the same reward probability. The sum of the weights of the presented images established the log of posterior odds and (by Bayes' rule) the log likelihood ratio (logLR) favoring one outcome over the other:

$$\text{logLR} = \log_{10}\frac{P(s_1,s_2,s_3,s_4|F)}{P(s_1,s_2,s_3,s_4|H)} = \sum_{i=1}^{4} w_i \qquad [1]$$

where s_i represents each of the four presented images and w_i the associated image weight. The logLR is often used as an aggregate representation of all incoming evidence (12, 30), and as such it determines reward probability. We therefore chose to evaluate behavioral performance as a function of logLR and to use logLR as an initial measure of identifying regions whose activity covaried with the likelihood of reward for each of the two alternatives.

Author contributions: M.G.P., G.B., and H.R.H. designed research; M.G.P. performed research; M.G.P. analyzed data; and M.G.P., G.B., and H.R.H. wrote the paper.

The authors declare no conflict of interest.

*This Direct Submission article had a prearranged editor.

[1]To whom correspondence should be addressed. E-mail: marios.philiastides@gmail.com.

This article contains supporting information online at www.pnas.org/lookup/suppl/doi:10.1073/pnas.1001732107/-/DCSupplemental.

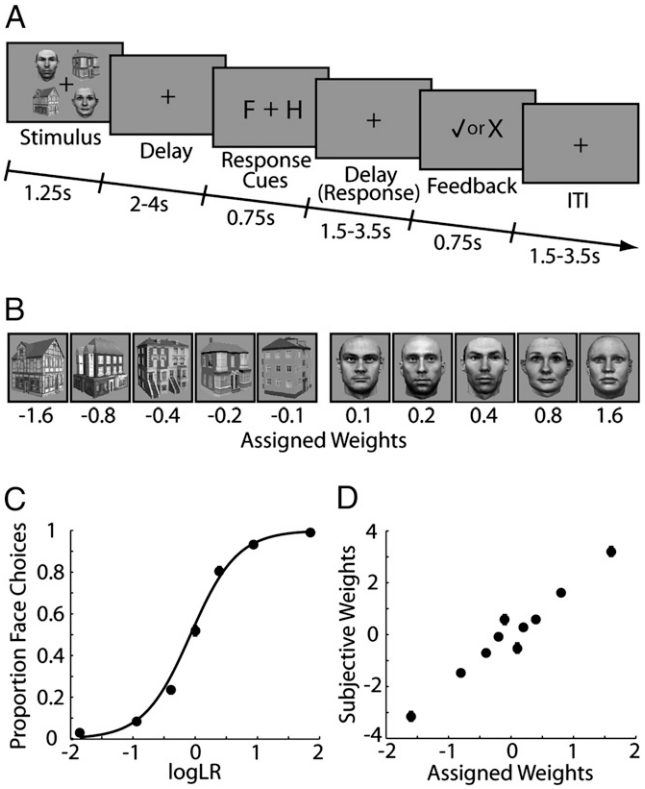

Fig. 1. Experimental task and behavioral performance. (*A*) Rapid-event-related fMRI design. Stimuli were presented for 1.25 s, and subjects responded with a button press after a forced delay (2–4 s). The response cue, which lasted for 750 ms, indicated the mapping between choice (face and house) and response hand (left and right). Subjects were instructed to respond after the response cue was extinguished and during a second delay period (1.5–3.5 s). Feedback (reward or not) was provided for 750 ms after the second delay. Intertrial interval (1.5–3.5 s) followed feedback. (*B*) The 10 images used in the task with their associated weights. On each trial the sum of the weights of the four presented images was used to manipulate reward probability. (*C*) Proportion of face choices as a function of logLR averaged across subjects. Trials were grouped into seven logLR bins. The sigmoidal curve is a logistic fit through the data. Individual responses depicted in Fig. S1*B*. (*D*) Average subjective weights plotted against the assigned weights. Individual estimates depicted in Fig. S1*C*. Error bars in *C* and *D* represent standard errors across subjects. For the most part, standard errors are smaller than the data points.

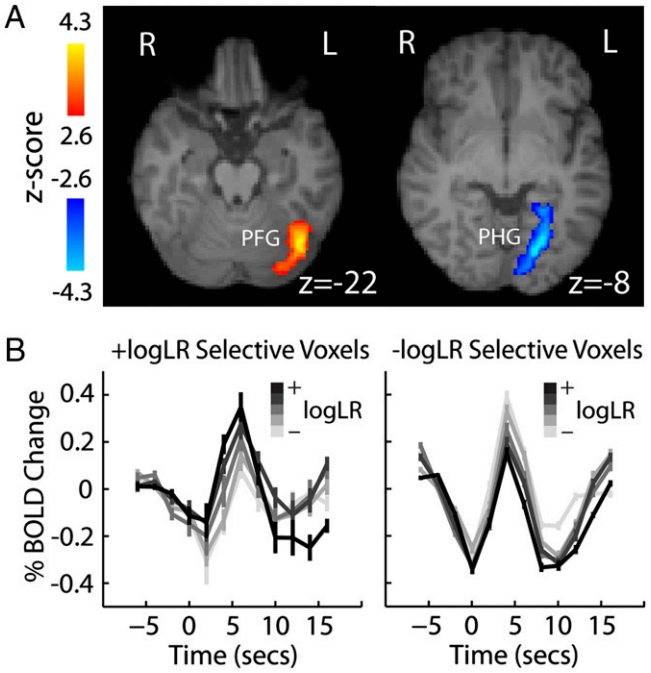

Fig. 2. Representation of probabilistic evidence in ventral temporal cortex. (*A*) A region in the left PFG [(*x* −40, *y* −70, *z* −20), *Z* = 4.13, peak Montreal Neurological Institute (MNI)] correlated positively with logLR (+logLR selective voxels), whereas a region in the left PHG [(*x* −20, *y* −74, *z* −8), *Z* = 4.28, peak MNI] correlated negatively with logLR (–logLR selective voxels). Activity in corresponding voxels in the right hemisphere showed a similar pattern but ultimately failed to survive our stringent significance tests. For visualization purposes images are thresholded at $Z > 2.6$ and $Z < -2.6$, respectively (uncorrected). Images are radiological convention. (*B*) Event-related BOLD signal averages (Eq. **10**) for five different logLR levels, from each of the two regions shown in *A*. Traces are aligned to the onset of visual stimulation at 0 s. The statistical contrast used to identify the regions (logLR) predetermined the shape of these plots, which are shown for illustrative purposes. Error bars represent SE across subjects.

After extensive training (*Materials and Methods* and *SI Methods*), subjects learned the rules of the task, and they based their choices on logLR by integrating all of the available evidence (*SI Results* and Fig. S1*A* for comparison with alternative choice models). Specifically, they chose face when logLR was large and positive and house when logLR was large and negative. For intermediate magnitudes of logLR, subjects chose both options but favored the one that was more likely to lead to a reward (Fig. 1*C* and Fig. S1*B*). To further assess the extent to which they learned each of the weights, we used logistic regression to compute subjective weights (Eq. **8** in *Materials and Methods*). The high correlation between the average subjective and assigned weights (Spearman's rank correlation, $r = 0.95$, $P < 10^{-6}$) reaffirmed that subjects learned the assigned weights well (Fig. 1*D* and Fig. S1*C*).

Our first objective was to test whether regions in the human ventral temporal cortex are sensitive to probabilistic evidence conferred by the different stimuli. We hypothesized that if there exist distinct neural populations that are activated by the likelihood of reward for each of the alternatives (face or house), then there should be voxels correlating either positively or negatively with a parametric logLR regressor (because logLR > 0 supports a face choice and logLR < 0 supports a house choice).

Indeed, we found the only activity that correlated significantly with the parametric logLR regressor in regions of the posterior fusiform gyrus (PFG; positive correlation, Fig. 2*A*, *Left*) and parahippocampal gyrus (PHG; negative correlation, Fig. 2*A*, *Right*). Both of these activations survived an additional cross-validation test (*SI Results* and Fig. S2 *A* and *B*). We obtained nearly identical results when we derived logLR from subjective weights. For illustrative purposes, Fig. 2*B* shows event-related blood oxygen level–dependent (BOLD) signal averages from each region, after grouping trials into five different logLR bins.

Given the proximity of these activations to face and house selective cortex, we tested to what extent activity in PFG and PHG reflected the amount of probabilistic evidence conferred by the two image categories separately. Note that these regions are close to but distinct from the fusiform face area (FFA) and parahippocampal place area (PPA) (which we identified in separate localizer scans; *SI Results* and Fig. S2 *C* and *D*) that have been shown to encode the sensory evidence associated with faces and houses (31, 32), respectively. We estimated the probabilistic weight of evidence for faces and houses (WOE_F and WOE_H, respectively) by taking the unsigned sum of weights for each presented pair of face and house images, respectively (*SI Methods* for additional discussion):

$$WOE_F \equiv w_{F1} + w_{F2} \quad [2]$$

$$WOE_H \equiv |w_{H1}| + |w_{H2}| \quad [3]$$

Note that the contrast $WOE_F - WOE_H$ is perfectly correlated with logLR. Crucially, this means that even if each region coded exclusively for either the face or house weight of evidence, the correlations with the logLR regressor would have been sufficient to identify these regions. The advantage of using separate representations for the probabilistic evidence provided by faces and houses was that it allowed us to investigate the influence of one representation on the activity identified by positive correlation with the other (i.e., to look at the signal change in response to WOE_H in voxels identified by WOE_F, and vice versa).

We reanalyzed our fMRI data by replacing the original logLR regressor with two new parametric regressors for WOE_F and WOE_H (note these regressors are orthogonal; Fig. S3*A*). In each of the PFG and PHG regions we identified clusters of voxels correlating positively with WOE_F and WOE_H, respectively. If each of these regions coded exclusively for the probabilistic evidence provided by each of the two categories, then the signal change in response to the opposing regressor should have been insignificant. Even though PFG and PHG encoded primarily the face and house weight of evidence, respectively (*SI Results* and Fig. S3*B*), they did not do so exclusively. Specifically, each of these regions also reduced its activity (relative to baseline) by a small but significant amount (one-tailed, t test, $P < 0.01$) in response to evidence supporting the alternative option (Fig. 3), suggestive of competitive interactions between the two regions (33).

Having established that regions in sensory cortex have the capacity to encode the probabilistic evidence conferred by the different decision alternatives, we turned to the question of how the brain uses this information to compute the value signal necessary to make the decision. Previous studies reported that value signals are represented in higher-level cortical regions, such as the medial prefrontal cortex (18–27). Crucially, however, those studies did not answer the question of whether these regions play an active role in computing these signals or whether they merely represent the consequence of the decision.

One hypothesis of how the brain might perform such computation entails that a higher-level region compares the output of sensory regions providing probabilistic evidence for each of the alternatives (here, PFG and PHG). This hypothesis stems from research on perceptual decision making in which single-unit recordings in primates and neuroimaging experiments in humans have shown that neural activity gradually increases in regions carrying out the comparison of sensory evidence, with a higher rate of increase for high than low sensory evidence, and then remains elevated until a response is made (16, 17).

If a similar mechanism is at work for computing decision value signals, then activity in candidate regions for carrying out this computation should correlate positively with a parametric regressor for the modulus of logLR (i.e., |logLR|)—that is, they should show a greater response for high logLR magnitude than for low logLR magnitude trials. In line with previous reports on perceptual decision making, we additionally required that a value-computing region should correlate with the trial-to-trial fluctuations in the absolute difference between the output signals of PFG and PHG. In contrast to the |logLR|, the absolute difference signal is expected to be a better predictor of the moment-to-moment changes in activity in value-computing regions because it reflects the neuronal response variability in regions encoding the probabilistic evidence for each of the decision alternatives (*SI Methods* for additional discussion).

Furthermore, using the absolute difference signal as a covariate addressed the confounding effects of task difficulty inherent in the |logLR| regressor (e.g., trials with higher logLR magnitude were generally less difficult). This is because the absolute difference signal also reflects the within-subject neuronal variability for repetitions of trials with the same logLR magnitude—that is, for trials that were equally difficult. Therefore, unlike the |logLR|, the trial-to-trial fluctuations in the absolute difference signal between PFG and PHG would not accurately predict activity covarying only with the overall difficulty of the task.

Activity in a number of regions correlated both positively and negatively with the |logLR| regressor. Activity in regions in the medial and ventromedial prefrontal cortex, the posterior cingulate cortex, and the amygdala/hippocampus was correlated positively with |logLR|. Activity in several brain regions typically associated with the human attentional network was negatively correlated with |logLR|. These regions, which included the frontal and supplementary eye fields, regions in the intraparietal sulcus, and the anterior insula, responded more strongly during more demanding low-magnitude logLR trials, which required more attentional resources for optimal performance (Table S1 shows a complete list of |logLR|-related activations).

To compute the difference between the activity of regions coding for face and house weight of evidence (i.e., PFG and PHG) we extracted, for each subject, time series data from WOE_F and WOE_H selective voxels. We then computed the absolute difference between the two time series (i.e., |PFG(t) – PHG(t)|) and identified voxels in which the BOLD signal

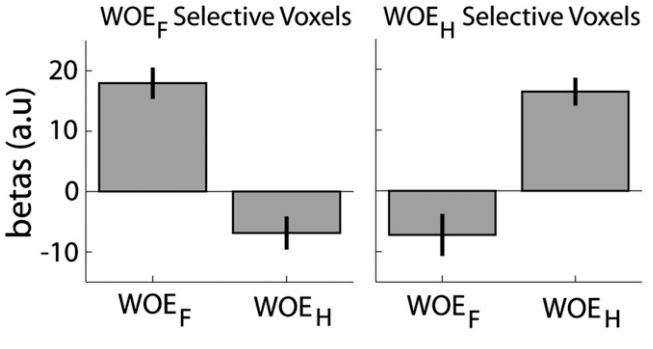

Fig. 3. Separate representation of WOE_F and WOE_H. Mean parameter estimates (βs) for the WOE_F and WOE_H regressors in voxels correlating positively with WOE_F (*Left*, WOE_F selective voxels) and WOE_H (*Right*, WOE_H selective voxels). These results demonstrate that activity in WOE_F and WOE_H selective voxels encoded primarily the face and house weight of evidence, respectively. Error bars represent SE across subjects.

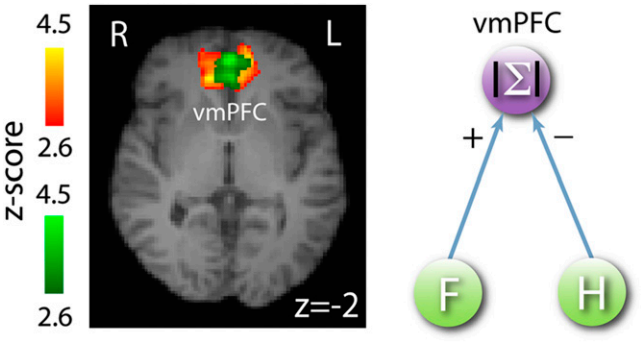

Fig. 4. Value signal computation in vmPFC. A region of the vmPFC covaried both with |logLR| [orange (x –6, y 50, z –2), $Z = 4.07$, peak MNI] and |PFG(t) – PHG(t)| [green (x –2, y 52, z –2), $Z = 4.45$, peak MNI], providing strong evidence that this region is involved in computing a value signal by combining the weight of evidence for face (F) and house (H) by using a difference-based comparator operation. For visualization purposes images are thresholded at $Z > 2.6$ (uncorrected). Images are radiological convention.

covaried with the resulting difference time course (see *Materials and Methods* for more details).

The only region in which changes in BOLD signal correlated positively with both the magnitude of logLR (i.e., |logLR|) and the absolute difference between the output of the regions representing face and house weight of evidence (i.e., |PFG(t) − PHG(t)|) was a region in the ventromedial prefrontal cortex (vmPFC) (Fig. 4). Additional control analyses (*SI Results*) confirmed that the BOLD activity in the vmPFC could not be explained either by changes in PFG and PHG alone (Fig. S4*A*) or by the absolute difference signal from regions encoding face and house sensory evidence (i.e., |FFA(t) − PPA(t)|; Fig. S4*B*). These findings strongly support the hypothesis that vmPFC is directly involved in computing the value signal by combining the different sources of probabilistic evidence using a simple subtraction operation.

Discussion

In recent years the study of the neurobiological and computational basis of value-based decision making has received considerable attention, and it has provided the foundation upon which the field of neuroeconomics was built. Despite recent progress in understanding the neural correlates of value-based decision making, two key questions, pertaining to how the brain represents different sources of probabilistic evidence and how it uses this information to compute value, still remain.

Nonsensory factors such as prior probability (34) and the presence of reward (9, 10) can influence early sensory representations. Recently, Serences (11) showed in a learning task that activity in the visual cortex is modulated by reward history (but not by reported subjective reward probabilities) and hypothesized that this signal could be used to bias choices. To date, it remains unclear, however, whether neural activity in distinct sensory regions is also modulated by the probabilistic evidence associated with different decision alternatives. Here, we show that during binary value-based decision making, distinct regions in human ventral temporal cortex (i.e., PFG and PHG) encode abstract probabilistic evidence conferred by each of the stimulus categories. Crucially, this is so even when the absolute amount of sensory evidence, per se, is equalized between the two categories.

An important question is how the modulation of the BOLD signal by the amount of probabilistic evidence in ventral temporal cortex is mediated. Reward and attention are intrinsically linked (35), and therefore one potential interpretation is that orienting attention to the more rewarding stimuli is the mechanism by which reward modulates sensory representations. Indeed, these top-down attention-orienting effects in relation to face and house stimuli have been reported previously for FFA and PPA but not for PFG and PHG (36). In the present study, however, the probabilistic evidence conferred by our stimuli did not modulate FFA and PPA, and the absolute difference in changes in BOLD signal between FFA and PPA did not covary with changes in BOLD signal in vmPFC (Fig. S4*B*). These findings thus render a purely attentional account of our results unlikely.

An alternative interpretation is that the effects observed in PFG and PHG are mediated through other brain regions. For instance, it has been suggested that individual neurons within reward-related structures that are heavily interconnected with both sensory and orbitofrontal cortex (e.g., amygdala) can form a plastic representation of the value of different visual stimuli (37, 38). This raises the possibility that our effects are mediated through neuronal subpopulations within these candidate regions. Future research based on single or multiunit recordings and/or high-resolution fMRI will be required to clarify this issue.

Despite previous reports implicating the medial prefrontal cortex in encoding expected value signals (18–27), it remained unclear whether this region is directly involved in computing value, because these signals are often thought to reflect the consequence of the decision process instead (in the sense that value can only be encoded once a decision has been made). In this work, we provide a mechanistic account that directly implicates the medial prefrontal cortex in value computation. Specifically, we show that a region in vmPFC is involved in computing decision value signals by integrating the different sources of probabilistic evidence encoded in ventral temporal cortex (i.e., PFG and PHG), using a difference-based comparator operation.

Importantly, this mechanism seems to be consistent with neurobiological and computational accounts already proposed for perceptual decision making (12, 15, 39, 40). Single-unit recordings in primates (16) and neuroimaging experiments in humans (13, 14) have shown that the dorsolateral prefrontal cortex (dlPFC) might be involved in forming a decision by comparing the output of lower-level regions that encode the sensory evidence for each of the perceptual choices, using a similar difference-based operation (41, 42). Even though the brain regions seem to be distinct (e.g., dlPFC and vmPFC), these results suggest that perceptual and value-based decision making might share a common neural mechanism.

Notably, our experimental design parallels that of Yang and Shadlen (30), who have trained animals to base their choices on the logLR favoring one outcome over another using a similar probabilistic categorization task. Confirming previous theoretical insights (12, 28, 43), they found that the build-up of activity in the lateral intraparietal area (LIP), leading to commitment to a behavioral choice, was proportional to logLR. Unlike Yang and Shadlen, however, we did not find any parietal activity (e.g., LIP) correlating with the absolute difference signal between PFG and PHG. This is most likely due to differences in the experimental design between the two studies. Specifically, we did not associate choices to eye movements, and we made sure that the decision was dissociated from the response by counterbalancing the mapping between choice and motor effectors (i.e., left/right index fingers) across trials. Instead, on the basis of whole-brain fMRI data, we offer a comprehensive account of the decision-making process including early representations of probabilistic evidence and calculation of decision value from these representations.

Although it remains to be seen how well this mechanism generalizes to other tasks using different stimulus material, our findings help advance the understanding of the neurobiological and computational basis of value-based decision making in humans and suggest a critical role of the vmPFC in integrating multiple sources of probabilistic information to guide behavior.

Materials and Methods

Participants. Twenty-two right-handed volunteers participated in the study (12 female; mean age, 25.3 years; range, 21–30 years). All had normal or corrected-to-normal vision and reported no history of neurological problems. Informed consent was obtained according to procedures approved by the local ethics committee of the Charité, University Medicine Berlin.

Visual Stimuli. Ten equiluminant grayscale images of faces (face database, Max Planck Institute for Biological Cybernetics, http://faces.kyb.tuebingen.mpg.de/) and houses (five per category) were used (image size: 128 × 150 pixels, 8 bits per pixel; mean luminance: 100). A Fujitsu Celsius H250 laptop computer with NVIDIA Quadro 570M graphics card and presentation software (Neurobehavioral Systems) controlled the stimulus display. Stimuli were presented by two small thin-film transistor monitors (resolution: 800 × 600 pixels; refresh rate: 60 Hz) mounted within the VisuaStim Digital goggle system (Resonance Technology). Each image was subtended 4.8° × 5.6°. The presentation software was interfaced with an MR compatible fiber optic response device (Cambridge Research Systems) to collect subject responses.

Probabilistic Categorization Task. A trial started with the presentation of four images (two faces and two houses pooled randomly, with replacement, from the set of 10 images) along with a central fixation cross. The position of the four images on the screen was assigned randomly on each trial. Images remained on the screen for 1,250 ms. Subjects decided whether a face or

a house choice was more likely to lead to a reward and responded with a button press after a forced delay (randomized in the range 2–4 s). A response cue, which followed the forced delay and lasted for 750 ms, indicated the mapping between the choice and the relevant motor effectors (i.e., left and right index fingers). The letters F (for face) and H (for house) placed randomly either to the left or to the right of the central fixation cross, established the mapping (e.g., if the letter F appeared to the left of the fixation cross and the participant decided that a face choice could lead to a reward then he/she should have pressed the left button). The position of the two letters was counterbalanced across trials. Subjects were instructed to respond after the response cue disappeared and during the next delay period, which lasted between 1.5 and 3.5 s. A feedback screen, which lasted for 750 ms, followed the delay and informed the subjects whether the trial was rewarded or not (with a check mark and a cross respectively). The trial ended with a variable intertrial interval, in the range 1.5–3.5 s. Fig. 1*A* outlines the order of these events. The experiment comprised 225 trials (three runs of 75 trials), which is the total number of possible combinations of the 10 images given the constraint that each trial always contained two faces and two houses. The sequence of events was optimized using a genetic algorithm as in ref. 44.

Reward on any given trial was not guaranteed, but it was instead determined probabilistically on the basis of the combination of weights assigned to the 10 images. Specifically, the sum of the weights associated with the four images presented on a given trial governed the probability that a face (F) or a house (H) choice would be rewarded:

$$P(F|s_1,s_2,s_3,s_4) = \frac{1}{1+10^{-\sum_{i=1}^{4} w_i}} \quad [4]$$

$$P(H|s_1,s_2,s_3,s_4) = 1 - P(F|s_1,s_2,s_3,s_4) \quad [5]$$

where s_i represents each of the four presented images and w_i the associated image weight. Reward was delivered using Eq. **4**. Subjects were told that they could earn anywhere between 25 and 50 Euros, depending on their performance. No further details regarding the mapping between rewarded trials and the final payout were given to the subjects (*SI Methods* for details on subject training). The weights were selected to support a reward rate for an ideal observer around 80% of trials, and they were as follows: $w_F = \{0.1 \quad 0.2 \quad 0.4 \quad 0.8 \quad 1.6\}$ for faces and $w_H = \{-0.1 \quad -0.2 \quad -0.4 \quad -0.8 \quad -1.6\}$ for houses. Weights were balanced between face and house images so that, on average, face and house choices shared the same probability of reward (i.e., $E[w] = E[\sum_{i=1}^{4} w_i] = 0$). This rule was observed even when partitioning the trials into individual runs.

Importantly, from Eq. **4** and Eq. **5** it follows that on any one trial the log of the posterior odds in favor of a face or a house choice equals the sum of the four weights. In addition, given equal prior face and house reward probabilities, Bayes' rule ensures that the sum of the four weights is also equal to the logLR favoring one outcome over the other:

$$\begin{aligned}\text{logLR} &= \log_{10}\frac{P(s_1,s_2,s_3,s_4|F)}{P(s_1,s_2,s_3,s_4|H)} = \log_{10}\frac{P(F|s_1,s_2,s_3,s_4)}{P(H|s_1,s_2,s_3,s_4)} \\ &= \sum_{i=1}^{4} w_i \end{aligned} \quad [6]$$

As such, the logLR is often thought of as an aggregate representation of all incoming information. In other words, logLR represents the impact that the stimuli have on the belief that a face or a house choice is correct. Accordingly, values near zero suggest that each choice has an approximately 50% chance of being rewarded, whereas deviations from zero indicate that either a face choice (if logLR > 0) or a house choice (if logLR < 0) has a higher chance (>50%) to lead to a reward. To investigate the individual influence of the two stimulus categories we also estimated the WOE conferred by faces and houses separately by taking the unsigned sum of weights for each presented pair of faces and houses (as in Eq. **2** and Eq. **3**; *SI Methods* for additional discussion). logLR, WOE_F, and WOE_H are therefore the main experimentally controlled independent variables in this study, and they are used as covariates in the various fMRI analysis schemes (see below).

Analysis of Behavioral Data. To describe behavioral performance the proportion of face choices was plotted against the logLR. Trials were grouped into seven logLR bins. Logistic regression was used to fit the seven data points with a sigmoid:

$$P_{face} = \frac{1}{1+10^{-K}} \text{ where } K = \beta_0 + \beta_1 \times \text{logLR}_{bin} \quad [7]$$

P_{face} denotes the proportion of face choices within a bin of trials, and logLR_{bin} the mean logLR within a bin of trials. This exercise was performed for the group average (Fig. 1*C*) and for the individual subjects (Fig. S1*B*).

To estimate the effect that each of the individual images had on the subjects' choices, a second logistic model was used to compute subjective weights as in ref. 30:

$$P_{face} = \frac{1}{1+10^{-K^*}} \text{ where } K^* = \sum_{j=1}^{10} w_j^* N_j \quad [8]$$

P_{face} is a vector of 1s and 0s indicating whether the subject chose face or not on each trial. N are the image counts shown in a trial. The 10 fitted coefficients, w_j^*, are the subjective weights and are used as a measure of how well subjects learned the task. This exercise was performed for the group average (Fig. 1*D*) and for the individual subjects (Fig. S1*C*).

fMRI Data Acquisition and Analysis. fMRI data acquisition, preprocessing, and registration were carried out using standard procedures described in *SI Methods*. Whole-brain statistical analyses of functional data were performed using a multilevel approach within the framework of a general linear model (GLM), as implemented in the FMRIB Software Library (45):

$$Y = X\beta + \varepsilon = \beta_1 X_1 + \beta_2 X_2 + + \beta_N X_N + \varepsilon \quad [9]$$

where Y is a $T\times1$ (T time samples) column vector containing the times series data for a given voxel, and X is a $T \times N$ (N regressors) design matrix with columns representing each of the psychological regressors convolved with a canonical hemodynamic response function (double-γ function). β is a $N \times 1$ column vector of regression coefficients (commonly referred to as parameter estimates) and ε a $T \times 1$ column vector of residual error terms. A first-level analysis was performed to analyze each subject's individual runs, which were then combined using a second-level analysis (fixed effects). Finally, to combine data across subjects a third-level, mixed-effects model was used (FLAME 1), treating participants as a random effect. Time series statistical analysis was carried out using FMRIB's improved linear model with local autocorrelation correction (46).

In total, we performed three different GLM analyses.

Identification of logLR sensitive regions. For this analysis we used seven main regressors to model the data during the stimulus presentation and decision phases of the experiment, as well as the response and feedback periods. Specifically, we used an unmodulated regressor (i.e., boxcar regressor with all event amplitudes set to 1) and two parametric regressors modulated by logLR and |logLR|, respectively, all with event onset times and duration matching that of the stimulus presentation. The amplitudes of these regressors ensured that they were uncorrelated. In addition, we used two unmodulated regressors for face and house choices, respectively, with event onset times and duration matching that of the response cue presentation, and two unmodulated regressors for rewarded and unrewarded trials, with event onset times and duration matching that of the feedback presentation. The contrasts [face – house] choices and [rewarded – unrewarded] trials were also computed.

Identification of WOE_F and WOE_H sensitive regions. In this analysis, two new parametric regressors, one for WOE_F and one for WOE_H, were used in place of the logLR regressor (same onset time and duration as the logLR regressor). By design, WOE_F and WOE_H were uncorrelated (Fig. S3*A*) and could therefore simultaneously appear in the same GLM design matrix. The remaining regressors were the same as in the first analysis. The contrast [WOE_F – WOE_H] was also added.

Identification of a comparator region. This analysis was used to identify voxels that correlated with the absolute difference between WOE_F and WOE_H selective voxels. The model also consisted of seven main regressors: an unmodulated regressor (as in the first analysis); a physiological regressor constructed by computing the absolute difference between the average time series (normalized data) of the voxels correlating with WOE_F and WOE_H in the second analysis, respectively; an interaction regressor between the unmodulated and physiological regressors; and two response and two feedback regressors as in the other two analyses. The interaction regressor was designed to reveal voxels that correlated with the absolute difference between WOE_F and WOE_H selective voxels, but only during the decision phase of the experiment.

In all three analyses, an additional, six nuisance regressors, one for each of the motion parameters (three rotations and three translations), were included in the design. We report clusters of maximally activated voxels that survived statistical thresholding at Z > 3.1 and had a minimum cluster size of 38 voxels estimated a priori with the afni AlphaSim tool (47).

Time Course Analysis of fMRI Data. To compute event-related BOLD signal averages (as percentage signal change) from predefined regions of interests, we defined a temporal window extending 6 s before to 16 s after event onset. We then estimated the BOLD signal traces for all events (trials) of a particular type as follows:

$$BOLD_j(t) = \left(\frac{X_j(t) - X_j^b}{\bar{X}}\right) \times 100 \qquad [10]$$

where j indexes trials, $X(t)$ is the event-locked data at time point t, X^b is the baseline signal defined as the average BOLD signal during the 6 s preceding each target event, and $\bar{X}$ the mean BOLD signal across all data points in a given run. Finally, traces across trials, runs, and subjects were averaged together.

ACKNOWLEDGMENTS. We thank Nils Bodammer and Sonali Beckmann for technical assistance and Paul Sajda and Leo Sugrue for comments on the manuscript. This work was supported by the Max Planck Society and the Deutsche Forschungsgemeinschaft (Emmy Noether Programme).

1. Schultz W (2006) Behavioral theories and the neurophysiology of reward. *Annu Rev Psychol* 57:87–115.
2. Montague PR, King-Casas B, Cohen JD (2006) Imaging valuation models in human choice. *Annu Rev Neurosci* 29:417–448.
3. Rangel A, Camerer C, Montague PR (2008) A framework for studying the neurobiology of value-based decision making. *Nat Rev Neurosci* 9:545–556.
4. Hare TA, Camerer CF, Rangel A (2009) Self-control in decision-making involves modulation of the vmPFC valuation system. *Science* 324:646–648.
5. Kable JW, Glimcher PW (2009) The neurobiology of decision: Consensus and controversy. *Neuron* 63:733–745.
6. Platt ML, Glimcher PW (1999) Neural correlates of decision variables in parietal cortex. *Nature* 400:233–238.
7. Sugrue LP, Corrado GS, Newsome WT (2004) Matching behavior and the representation of value in the parietal cortex. *Science* 304:1782–1787.
8. Kim S, Hwang J, Lee D (2008) Prefrontal coding of temporally discounted values during intertemporal choice. *Neuron* 59:161–172.
9. Krawczyk DC, Gazzaley A, D'Esposito M (2007) Reward modulation of prefrontal and visual association cortex during an incentive working memory task. *Brain Res* 1141: 168–177.
10. Pleger B, Blankenburg F, Ruff CC, Driver J, Dolan RJ (2008) Reward facilitates tactile judgments and modulates hemodynamic responses in human primary somatosensory cortex. *J Neurosci* 28:8161–8168.
11. Serences JT (2008) Value-based modulations in human visual cortex. *Neuron* 60: 1169–1181.
12. Gold JI, Shadlen MN (2007) The neural basis of decision making. *Annu Rev Neurosci* 30:535–574.
13. Heekeren HR, Marrett S, Bandettini PA, Ungerleider LG (2004) A general mechanism for perceptual decision-making in the human brain. *Nature* 431:859–862.
14. Heekeren HR, Marrett S, Ruff DA, Bandettini PA, Ungerleider LG (2006) Involvement of human left dorsolateral prefrontal cortex in perceptual decision making is independent of response modality. *Proc Natl Acad Sci USA* 103:10023–10028.
15. Heekeren HR, Marrett S, Ungerleider LG (2008) The neural systems that mediate human perceptual decision making. *Nat Rev Neurosci* 9:467–479.
16. Kim JN, Shadlen MN (1999) Neural correlates of a decision in the dorsolateral prefrontal cortex of the macaque. *Nat Neurosci* 2:176–185.
17. Shadlen MN, Newsome WT (2001) Neural basis of a perceptual decision in the parietal cortex (area LIP) of the rhesus monkey. *J Neurophysiol* 86:1916–1936.
18. Gläscher J, Hampton AN, O'Doherty JP (2009) Determining a role for ventromedial prefrontal cortex in encoding action-based value signals during reward-related decision making. *Cereb Cortex* 19:483–495.
19. Hampton AN, O'doherty JP (2007) Decoding the neural substrates of reward-related decision making with functional MRI. *Proc Natl Acad Sci USA* 104:1377–1382.
20. Hampton AN, Bossaerts P, O'Doherty JP (2006) The role of the ventromedial prefrontal cortex in abstract state-based inference during decision making in humans. *J Neurosci* 26:8360–8367.
21. Daw ND, O'Doherty JP, Dayan P, Seymour B, Dolan RJ (2006) Cortical substrates for exploratory decisions in humans. *Nature* 441:876–879.
22. Knutson B, Taylor J, Kaufman M, Peterson R, Glover G (2005) Distributed neural representation of expected value. *J Neurosci* 25:4806–4812.
23. Blair K, et al. (2006) Choosing the lesser of two evils, the better of two goods: Specifying the roles of ventromedial prefrontal cortex and dorsal anterior cingulate in object choice. *J Neurosci* 26:11379–11386.
24. Kable JW, Glimcher PW (2007) The neural correlates of subjective value during intertemporal choice. *Nat Neurosci* 10:1625–1633.
25. Fellows LK, Farah MJ (2007) The role of ventromedial prefrontal cortex in decision making: judgment under uncertainty or judgment per se? *Cereb Cortex* 17: 2669–2674.
26. Chib VS, Rangel A, Shimojo S, O'Doherty JP (2009) Evidence for a common representation of decision values for dissimilar goods in human ventromedial prefrontal cortex. *J Neurosci* 29:12315–12320.
27. FitzGerald TH, Seymour B, Dolan RJ (2009) The role of human orbitofrontal cortex in value comparison for incommensurable objects. *J Neurosci* 29:8388–8395.
28. Gold JI, Shadlen MN (2001) Neural computations that underlie decisions about sensory stimuli. *Trends Cogn Sci* 5:10–16.
29. von Neumann J, Morgenstern O (1944) *Theories of Games and Economic Behavior* (Princeton Univ Press, Princeton).
30. Yang T, Shadlen MN (2007) Probabilistic reasoning by neurons. *Nature* 447: 1075–1080.
31. Kanwisher N, McDermott J, Chun MM (1997) The fusiform face area: A module in human extrastriate cortex specialized for face perception. *J Neurosci* 17:4302–4311.
32. Epstein R, Kanwisher N (1998) A cortical representation of the local visual environment. *Nature* 392:598–601.
33. Kastner S, De Weerd P, Desimone R, Ungerleider LG (1998) Mechanisms of directed attention in the human extrastriate cortex as revealed by functional MRI. *Science* 282: 108–111.
34. Sharma J, Dragoi V, Tenenbaum JB, Miller EK, Sur M (2003) V1 neurons signal acquisition of an internal representation of stimulus location. *Science* 300:1758–1763.
35. Maunsell JH (2004) Neuronal representations of cognitive state: Reward or attention? *Trends Cogn Sci* 8:261–265.
36. Gazzaley A, Cooney JW, McEvoy K, Knight RT, D'Esposito M (2005) Top-down enhancement and suppression of the magnitude and speed of neural activity. *J Cogn Neurosci* 17:507–517.
37. Paton JJ, Belova MA, Morrison SE, Salzman CD (2006) The primate amygdala represents the positive and negative value of visual stimuli during learning. *Nature* 439:865–870.
38. Gottfried JA, O'Doherty J, Dolan RJ (2003) Encoding predictive reward value in human amygdala and orbitofrontal cortex. *Science* 301:1104–1107.
39. Bogacz R (2007) Optimal decision-making theories: Linking neurobiology with behaviour. *Trends Cogn Sci* 11:118–125.
40. Ratcliff R, Smith PL (2004) A comparison of sequential sampling models for two-choice reaction time. *Psychol Rev* 111:333–367.
41. Shadlen MN, Britten KH, Newsome WT, Movshon JA (1996) A computational analysis of the relationship between neuronal and behavioral responses to visual motion. *J Neurosci* 16:1486–1510.
42. Mazurek ME, Roitman JD, Ditterich J, Shadlen MN (2003) A role for neural integrators in perceptual decision making. *Cereb Cortex* 13:1257–1269.
43. Jazayeri M, Movshon JA (2006) Optimal representation of sensory information by neural populations. *Nat Neurosci* 9:690–696.
44. Wager TD, Nichols TE (2003) Optimization of experimental design in fMRI: A general framework using a genetic algorithm. *Neuroimage* 18:293–309.
45. Smith SM, et al. (2004) Advances in functional and structural MR image analysis and implementation as FSL. *Neuroimage* 23 (Suppl 1):S208–S219.
46. Woolrich MW, Ripley BD, Brady M, Smith SM (2001) Temporal autocorrelation in univariate linear modeling of FMRI data. *Neuroimage* 14:1370–1386.
47. Ward BD (2000) Simultaneous inference for FMRI data. Available at: http://afni.nimh.nih.gov/pub/dist/doc/manual/AlphaSim.pdf.

Supporting Information

Philiastides et al. 10.1073/pnas.1001732107

SI Methods

Subject Training. Subjects were not explicitly told the weight assignments for the 10 images. Instead, they were initially trained on a two-image version of the probabilistic categorization task to implicitly learn the relative associations between images. Each trial comprised one face and one house image, and subjects were asked to select the option (face or house) that was more likely to lead to reward. Reward was given probabilistically using Eq. **4** in the main text. The sequence of events was identical to those used in the main, four-image version of the experiment. Training on the two-image version of the task terminated when subjects achieved above 80% correct choices and after they had completed at least 400 trials. A correct choice here is referred to as the one that was favored by the odds, regardless of whether it was rewarded. Subjects were then trained on the four-image version of the task until they reached above 75% correct choices and after they had completed at least 300 trials. The day of the functional magnetic resonance imaging (fMRI) scanning session, subjects completed an additional 75 trials on the two-image version of the task. The fMRI session was always scheduled within 2 to 3 days of the training session.

MRI Data Acquisition. Whole-brain fMRI data were collected on a 3T Siemens Magnetom Trio scanner using a 12-channel phased-array head coil. Echoplanar images (EPI) were acquired from 36 axial slices of 68 × 68 voxels with 3-mm in-plane resolution, 3.45-mm slice thickness, field of view (FOV) of 204 mm, 80° flip angle, 28-ms echo time (TE), and 2-s repetition time (TR). For each participant three runs of 429 volumes each were acquired. For all runs the first nine volumes were discarded to allow for magnetization equilibration. Initial scout scans were performed to localize slice planes parallel to the anterior commissure–posterior commissure line. In addition, high-resolution T1-weighted structural scans were collected for each participant for registration purposes using an MPRAGE sequence (192 sagittal slices; matrix size: 256 × 256; voxel size: 1 × 1 × 1 mm; FOV: 256 mm; flip angle: 9°; TE: 2.52 ms; TR: 1.9 s).

fMRI Data Preprocessing and Registration. Initial fMRI data preprocessing was performed using the FMRIB's Software Library (1, 2) and included head motion correction, slice-timing correction, high-pass filtering (>50 s), and spatial smoothing (with a Gaussian kernel of 6 mm full-width at half maximum). Registration of EPI images to standard space (Montreal Neurological Institute, MNI) was performed using FMRIB's Linear Image Registration Tool (3). To make registration as consistent across runs as possible, a three-step procedure was used. EPI images from each run were first registered to a common EPI space (typically the EPI image of the middle run). Then all EPI images were registered to individual high-resolution space. Both of these steps involved a six-parameter rigid body transformation. Finally, registration to standard space was carried out by a 12-parameter affine transformation.

Estimating Face and House Weight of Evidence. To investigate the individual influence of the two stimulus categories, we estimated the weight of evidence (WOE) conferred by faces and houses separately by taking the unsigned sum of weights for each presented pair of faces and houses (as in Eqs. **2** and **3** in the main text).

Note, however, that estimating the probabilistic evidence provided from a subset of our presented images using the partial sum of weights assumes that the probabilities of observing the remaining images are conditionally independent. This assumption, however, can be violated given knowledge that, on any one trial, reward is definitely associated with a face or a house choice.

An alternative measure of face and house WOE that accounts for these conditional dependencies can be derived by estimating the log likelihood ratios from partial—face or house—evidence. Given equal face and house prior reward probabilities and equal prior probabilities of observing each of the four image combinations, we can approximate the partial log likelihood ratios (logLRs) by tabulating the expected frequencies of reward associated with each pair of images:

$$\mathrm{WOE'_F} \equiv \log_{10}\frac{P(s_{F1},s_{F2}|F)}{P(s_{F1},s_{F2}|H)} \equiv \log_{10}\frac{\sum_{i,j}P\left(F|s_{F1},s_{F2},s_{Hi},s_{Hj}\right)}{\sum_{i,j}P\left(H|s_{F1},s_{F2},s_{Hi},s_{Hj}\right)} \quad \textbf{[S1]}$$

$$\mathrm{WOE'_H} \equiv \log_{10}\frac{P(s_{H1},s_{H2}|H)}{P(s_{H1},s_{H2}|F)} \equiv \log_{10}\frac{\sum_{i,j}P\left(H|s_{Fi},s_{Fj},s_{H1},s_{H2}\right)}{\sum_{i,j}P\left(F|s_{Fi},s_{Fj},s_{H1},s_{H2}\right)} \quad \textbf{[S2]}$$

where $s_{F1,2}$ and $s_{H1,2}$ are a given pair of face and house stimuli, respectively, and the summations are performed over all possible pairs (i, j) of houses (Eq. **S1**) and faces (Eq. **S2**).

As expected, $\mathrm{WOE'_F}$ and $\mathrm{WOE'_H}$ were a linear combination of $\mathrm{WOE_F}$ and $\mathrm{WOE_H}$ (i.e., they were very highly correlated), and the results of all analyses involving these quantities remained unchanged regardless of the method used to derive them. Given the complexity of estimating partial logLRs, and that partial logLRs are more pertinent when images are presented sequentially, it is reasonable to assume that in this case the brain uses a simpler quantity, such as the partial sum of weights, to estimate face and house WOE.

Identifying Regions Involved in Value Computation. In the main text we highlighted the importance of using the absolute difference signal between posterior fusiform gyrus (PFG) and parahippocampal gyrus (PHG) (i.e., |PFG(t) − PHG(t)|) as a regressor in our fMRI analysis to identify regions involved in value computation. Here, we provide additional insights as to why this regressor could provide a better estimate of the underlying neural activity than the |logLR| regressor. By using the normalized time series difference regressor, we capitalized on different sources of, across- and within-subject neuronal response variability in the brain regions tuned to the face and house weight of evidence, respectively (i.e., PFG and PHG).

First, we took advantage of the across-subject variability in the estimates of the assigned weights (Fig. S1*C*). When using the logLR magnitude as a regressor, we assumed that all participants used the same face and house weight of evidence to make a choice. In contrast, subjective assessments of the face and house weight of evidence could deviate somewhat, across participants, from their objective (i.e., experimentally defined) counterparts. Using the absolute time series difference from PFG and PHG as a regressor implicitly took into account these interindividual differences.

Another source of variability originated from trials where repetitions of the same stimuli occurred (due to inherent trial-to-trial fluctuations in neural processing), whereas a third source came from repetitions of trials with the same task difficulty—that is, trials with the same logLR magnitude (note, however, that repetitions of unique logLR magnitudes originated from different combinations of face and house stimuli). As highlighted in the main text,

this source of variability could also be used to address potential task difficulty effects associated with the |logLR| regressor.

Importantly, what all of these sources of variability have in common is that they all could result in trial-to-trial fluctuations in the absolute difference signal between PFG and PHG. That is ultimately why we required that areas involved in value computation (by comparing the output of sensory regions providing probabilistic evidence for each of the alternatives) should correlate with the trial-to-trial fluctuations in the absolute difference signal between PFG and PHG.

SI Results

Comparison of Different Behavioral Models. To ascertain the effect of the different image combinations on choice and to provide more compelling evidence that it is the integration of the overall weight of evidence (i.e., logLR) that governs choice, we tested a variety of behavioral models.

For each model we fit the behavioral data using the following logistic formulation:

$$P_{face} = \frac{1}{1 + 10^{-K}} \text{ where } K = \beta_0 + \beta_1 \times Q \qquad \text{[S3]}$$

where the independent variable, Q, is determined by the assumptions of each model (see below). P_{face} is a vector of 1s and 0s indicating whether the subject chose face or not on any given trial. Importantly, the fits are performed on each subject separately (as opposed to across an aggregate representation of all subjects).

The first model assumed that subjects based their choices on the overall weight of evidence as measured by logLR (i.e., $Q = \Sigma(w_{1-4}) = \text{logLR}$). The second model assumed that subjects based their decisions only on the most significant face and house images [i.e., ignore the lowest face and house weights, $Q = \text{best}(w(F)) + \text{best}(w(H))$]. The third and fourth models assumed that subjects tracked the probabilistic evidence provided by either faces or houses, respectively, while ignoring the weight of evidence provided by the opposite stimulus category [i.e., $Q = \Sigma(w(F))$ and $Q = \Sigma(w(H))$, respectively]. The rationale for the latter two models was that subjects might have interpreted evidence for one category as representing (simultaneously) evidence against the other.

To compare the goodness of fit for each model, we used the Akaike information criterion (AIC) and the Bayesian information criterion (BIC) resulting from each analysis:

$$AIC = -2\ln(L) + 2d \qquad \text{[S4]}$$

$$BIC = -2\ln(L) + d\ln(N) \qquad \text{[S5]}$$

where $\ln(L)$ is the maximized log likelihood of the observations in P_{face} with respect to the estimated model (assuming the Bernoulli distribution of binary choices), d the difference in the number of parameters between models and N the total number of trials. Results are summarized in Fig. S1*A* and clearly demonstrate that the model that assumed choices were based on the overall weight of evidence (i.e., logLR) described our subjects' behavior best.

Cross-Validating the Main Effects of logLR. As an additional test of significance for the main effects of logLR, we used a simple cross-validation procedure. Specifically, we setup a new general linear model (GLM) analysis with four regressors: an unmodulated regressor for all trials with positive logLR values, an unmodulated regressor for all trials with negative logLR values, and two unmodulated regressors to absorb the variance of the response and feedback periods. The contrast between the first two regressors was used to identify +logLR and −logLR selective regions. Importantly, for this we only used a subset of the data (training set)—from the first and last (third) runs. The effects were then retested (on the voxels identified in the training set) using the remaining (second) run and found to remain significant. Fig. S2 *A* and *B* summarize these results.

FFA and PPA Functional Localizer Scans. To identify face and house selective voxels in ventral temporal cortex [i.e., fusiform face area (FFA) and parahippocampal place area (PPA)], we used two separate functional localizer runs. During the first run (block design), subjects passively viewed 10 alternating blocks of clear (unmodulated), unmasked face and house images. Stimuli were presented for 750 ms with 250-ms interstimulus intervals, in blocks of 16 consecutive stimuli. A 12-s rest period was interleaved between blocks. The second run (event-related design) was designed so that the different trial events were identical to those used in the main task (i.e., image presentation, delay, response cue, delay, feedback, and intertrial interval). Subjects were once again presented with four images (arranged as in the main task) with the exception that two of the images were either clear faces or clear houses, whereas the remaining two were random phase (scrambled) images (of the same size and luminance as the clear images). Subjects had to report whether the clear images depicted faces or houses. There was a total of 40 face and 40 house trials. A set of 40 previously unseen face and house images was used for these localizer runs. All random phase images had an identical magnitude spectrum (average magnitude spectrum of the original face and house stimuli) and random phase spectra.

We used the same MRI acquisition parameters as in the main experiment, and for each of the block and event-related designs we collected data from single runs of 156 and 450 volumes, respectively. The fMRI data preprocessing was identical to that used in the main experiment. For both functional localizers the GLM analysis included two unmodulated regressors—one for face and one for house trials. For the event-related design two additional unmodulated regressors were included to absorb the variance of the response and feedback periods. In both cases the contrast [faces − houses] was used to identify face and house selective voxels (Fig. S2 *C* and *D*). Significance was determined as in the main experiment.

Separate Representation of Face and House WOE. To provide further support that the activations in PFG and PHG primarily encode the face and house weight of evidence, respectively, we examined trials with values of logLR near zero. Specifically, such trials arose when there was either low evidence for both faces and houses or high evidence for both faces and houses. We therefore separated all trials with logLR around zero ($|\text{logLR}| \leq 0.1$) into those with low and high WOE_F (for the PFG activation) and those with low and high WOE_H (for the PHG activation) and computed event-related blood oxygen level–dependent (BOLD) signal averages. At the peak of the hemodynamic response (for each of the PFG and PHG activations), activity for trials with high weight of evidence was significantly higher than for trials with low weight of evidence (one-tailed, paired t test, $P < 0.01$) (Fig. S3*B*), indicating that PFG and PHG respond primarily as a function of the face and house weight of evidence, respectively.

Testing for Individual PFG and PHG Effects on vmPFC. To provide further support that activity in the ventromedial prefrontal cortex (vmPFC) covaried uniquely with the absolute difference signal between PFG and PHG, we performed additional control analyses testing whether the individual responses from these regions (i.e., PFG and PGH) could also drive the vmPFC. To perform these analyses we used the times series data from these regions [i.e., PFG(t) and PHG(t)] as covariates in a GLM analysis.

Specifically, our GLM design matrix contained the following regressors: a physiological regressor constructed by averaging the time series (normalized data) of the voxels in PFG (or PHG), a

psychological regressor indicating subject choices, and an interaction regressor between the two (i.e., [PFG(t) or PHG(t)] × Choice [F = 1, H = −1, for PFG(t) and F = −1, H = 1, for PHG(t)]). Similar to the main analyses presented in *Materials and Methods*, we also included unmodulated regressors to absorb the variance of the early visual response, and feedback periods of the experiment.

To investigate whether BOLD activity in the vmPFC correlated with activity in regions encoding the probabilistic evidence for faces and houses alone, we relied on the regressors resulting from the interaction of PFG(t) and PHG(t) with choice. Fig. S4*A* shows the unthresholded *Z*-value maps associated with these regressors. We found no activation surpassing our thresholding criteria for significance ($Z > 3.1$ uncorrected, cluster size = 38 voxels) in the prefrontal cortex. These results provided further support that activity in vmPFC covaried only with the absolute difference signal between these regions.

Testing for |FFA(t) − PPA(t)| Correlation with vmPFC. To further ensure that the vmPFC covaried with the absolute difference signal between regions encoding probabilistic evidence (e.g., PFG and PHG), we performed another control analysis. Specifically, we repeated the GLM analysis designed to identify a comparator region by replacing the absolute difference signal between PFG and PHG with that of regions encoding face and house sensory evidence instead (i.e., FFA and PPA). Time series data for these regions were extracted from face and house selective voxels as identified by the functional localizer scans.

Fig. S4*B* shows that vmPFC did not correlate significantly with the absolute difference signal between FFA and PPA, indicating that this region of the prefrontal cortex integrates information only from regions encoding probabilistic evidence required to make a value-based decision. This result also reinforced the notion that PFG and PHG are functionally distinct from face and house selective regions that encode the amount of sensory evidence instead.

1. Smith SM, et al. (2004) Advances in functional and structural MR image analysis and implementation as FSL. *Neuroimage* 23 (Suppl 1):S208–S219.
2. Woolrich MW, et al. (2009) Bayesian analysis of neuroimaging data in FSL. *Neuroimage* 45 (1 Suppl):S173–S186.
3. Jenkinson M, Smith S; S3 (2001) A global optimisation method for robust affine registration of brain images. *Med Image Anal* 5:143–156.

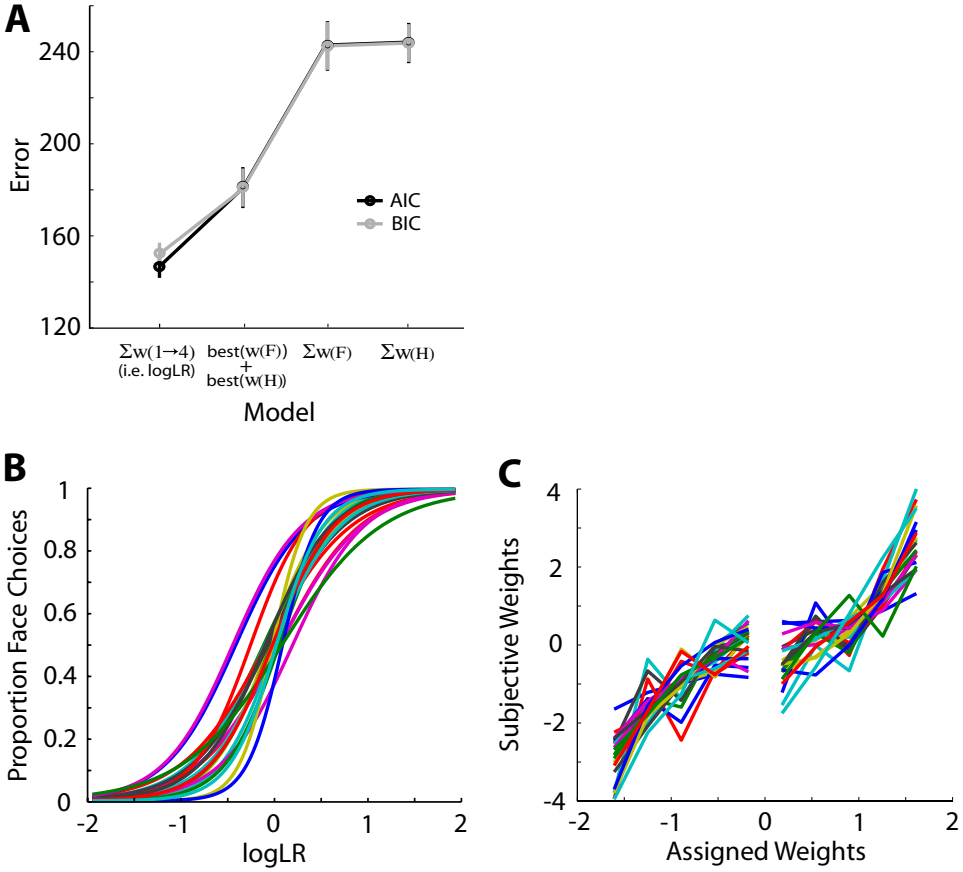

Fig. S1. Comparing different models of behavioral choice and behavioral performance of individual subjects. (*A*) We evaluated four different models of behavioral choice. The first model assumed that subjects based their choices on the overall weight of evidence (i.e., logLR). The second model assumed that subjects based their decisions only on the most significant face and house images. The third and fourth models assumed that subjects tracked exclusively the probabilistic evidence provided by faces or houses, respectively, while ignoring the weight of evidence provided by the opposite stimulus category. We used these models to fit the actual choices made by our subjects (on a subject-by-subject basis). We evaluated the goodness of fit for each model using the AIC and BIC criteria. The model that assumed choices were based on logLR fit the subjects' responses best. Error bars represent SE across subjects. (*B*) Proportion of face choices plotted as a function of logLR—trials grouped into seven logLR bins. The sigmoidal curves are logistic fits through the data (Eq. **7** in *Materials and Methods*). (*C*) Subjective weights (estimated using Eq. **8** in *Materials and Methods*) as a function of the assigned weights. Although there is some variance across participants, the rank ordering of the subjective weights (Spearman's rank correlation test, 19 subjects $P < 5 \times 10^{-3}$, 3 subjects $P < 0.05$) suggests that all subjects learned the rules of the task well.

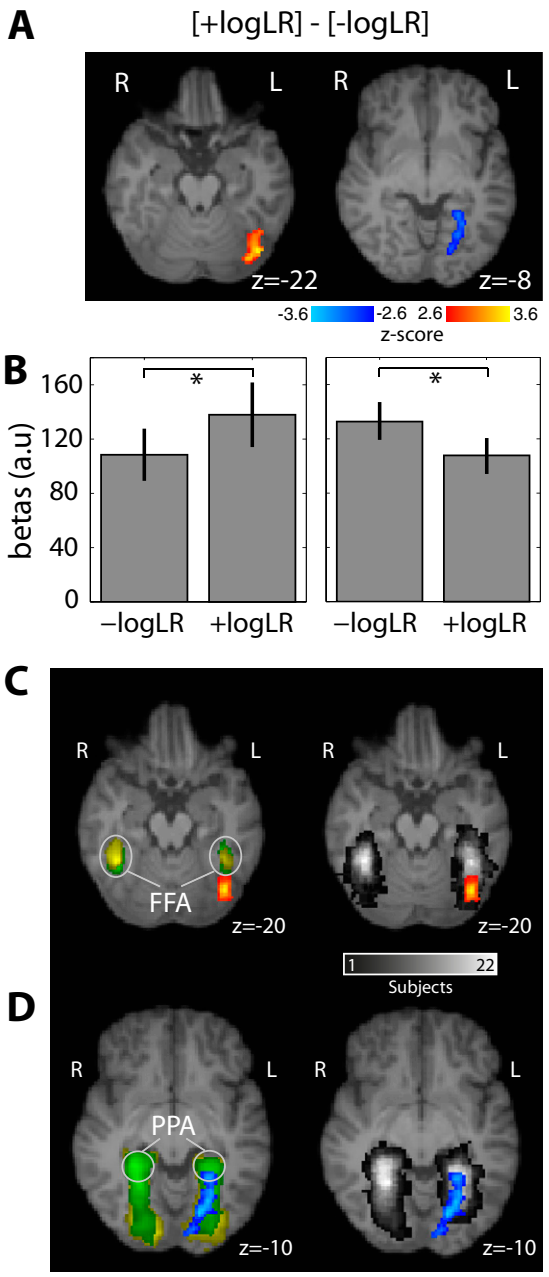

Fig. S2. Cross-validating the main effects of logLR and comparison with functional localizers. (*A*) We identified regions that correlated more with +logLR trials than −logLR trials (orange) and vice versa (blue) using a subset of the fMRI data (first and third runs) as training set. Note the clear resemblance of these activations to those identified using the parametric logLR regressor in Fig. 2*A* in the main text. For visualization purposes images are thresholded at $Z > 2.6$ and $Z < -2.6$, respectively (uncorrected). Images are radiological convention. (*B*) We retested the effects between +logLR and −logLR using the fMRI data from the second (test) run. Specifically, the mean parameter estimates (across subjects) for +logLR and −logLR were extracted from voxels identified in the training set. In +logLR selective voxels (*Left*), parameter estimates for +logLR were significantly higher than those of −logLR (one-tailed, paired *t* test, $P < 0.01$) and in −logLR selective voxels (*Right*), parameters estimates for −logLR were significantly higher than those of +logLR (one-tailed, paired *t* test, $P < 0.01$), confirming the significance of the main effects. (*C* and *D*) We used two separate functional localizers (block and event-related designs) to identify (*C*) face and (*D*) house selective regions (including the FFA and PPA) in the ventral temporal cortex ($Z > 3.1$, uncorrected). Green and yellow activations represent group results from the block and even-related designs, respectively. Note the striking similarity between the activations resulting from the two localizers. Also note the right face bias reported previously [Kanwisher N, McDermott J Chun MM (1997) The fusiform face area: A module in human extrastriate cortex specialized for face perception. *J Neurosci* 17:4302–4311]. Identifying the face and house selective voxels in each subject separately (in the event-related design), binarizing the resulting activation maps, and summing across subjects produced the grayscale "activations" seen on the right. A voxel value of 22 indicates that voxel was activated in all subjects. This exercise provided a convenient means of visualizing the across-subject variability seen in these areas. The main effects of logLR in PFG (orange) and PHG (blue) are superimposed for comparison purposes. It appears as though these regions are distinct from areas implicated in processing faces and houses (e.g., FFA and PPA), as identified by the functional localizers. For visualization purposes images are thresholded at $Z > 2.6$ (uncorrected). Images are radiological convention.

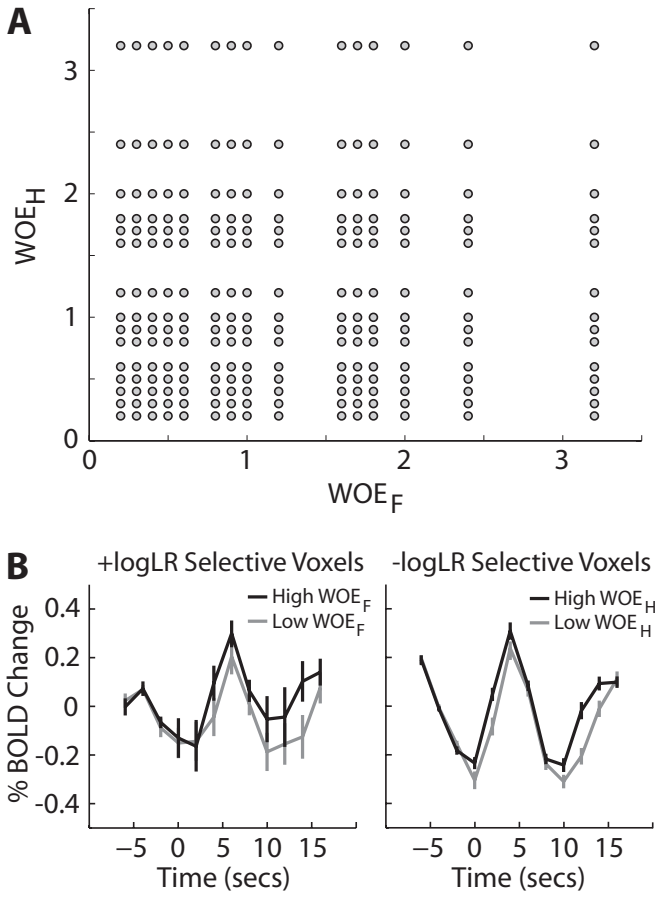

Fig. S3. Scatter plot of the face vs. house weight of evidence and their effect on low logLR trials. (*A*) The values of WOE_F and WOE_H were taken from the trials used in the main experiment. As can be seen from the scatter plot the parametric regressors resulting from these quantities were orthogonal. (*B*) Event-related BOLD averages in +logLR and −logLR selective voxels (as identified by the logLR regressor) but for trials with logLR values near zero ($|logLR| \leq 0.1$). Trials were further divided into high (black) and low (gray) face weight of evidence (in +logLR voxels, *Left*) and into high (black) and low (gray) house weight of evidence (in −logLR voxels, *Right*). Error bars represent standard errors across subjects.

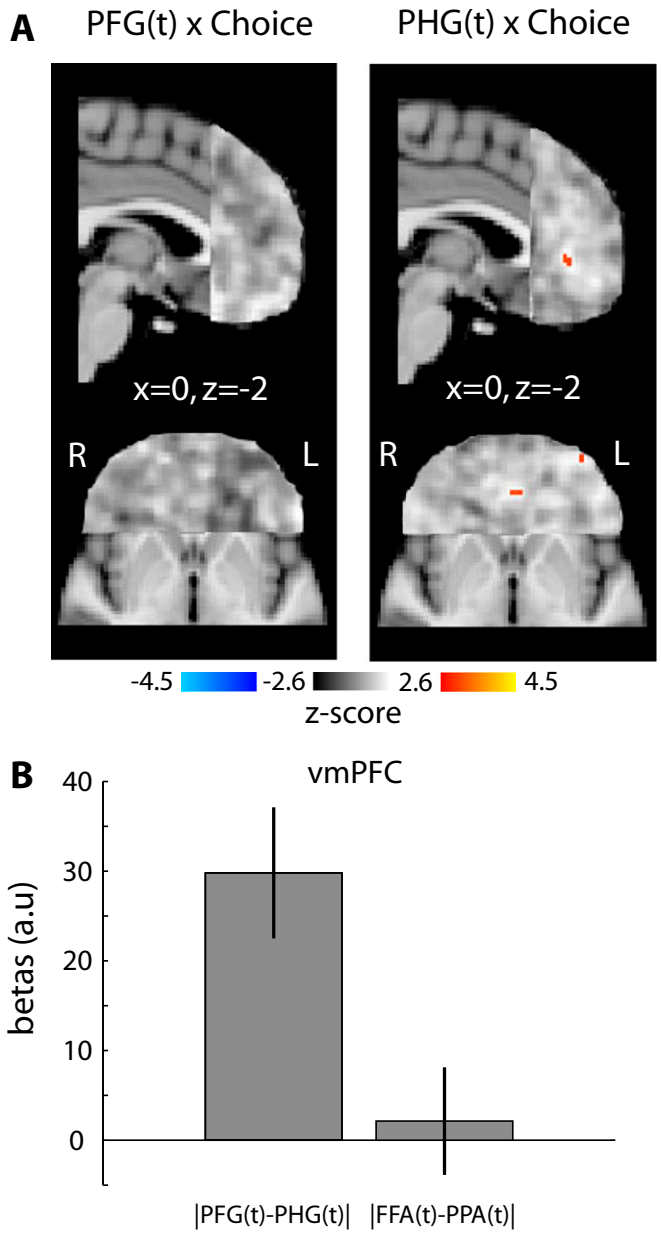

Fig. S4. Testing for individual PFG and PHG effects on vmPFC and for |FFA(t) − PPA(t)| correlation with vmPFC. (*A*) To control for the possibility that BOLD activity in the vmPFC might show a correlation with the activation in PFG and PHG alone, we looked at the psychophysical interaction between the time series data from these regions and subjects' choices [i.e., PFG(t) × Choice and PHG(t) × Choice]. Images show unthresholded *Z*-value maps of the prefrontal cortex for each of the two interactions. We found no activation surpassing our thresholding criteria for significance ($Z > 3.1$ uncorrected, cluster size = 38 voxels), indicating that neither PFG nor PHG can drive the vmPFC alone. (*B*) To ensure that the vmPFC covaried with the absolute difference signal between regions encoding only probabilistic evidence, we looked at the signal change in this region in response to the absolute difference signal between regions encoding sensory evidence instead [i.e., |FFA(t) − PPA(t)|]. The signal change in the vmPFC in response to |FFA(t) − PPA(t)| was insignificant, indicating that this region only integrates information from regions encoding probabilistic evidence. Error bars represent standard errors across subjects.

Table S1. Complete list of activations correlating positively with the parametric |logLR| regressor used in the first main analysis of the fMRI data

Brain region	BA	Hemisphere	Peak MNI coordinates (mm)			*Z* value (peak)
			x	*y*	*z*	
Superior frontal gyrus	9	R	14	54	30	5.02
		L	−16	56	28	6.01
Medial frontal gyrus	9	R	4	56	12	3.77
		L	−6	62	12	5.35
	10	R	8	52	2	4.30
		L	−10	52	−2	4.85
Anterior cingulate cortex (ventral)	24/32	R	10	40	−2	4.89
		L	−6	42	0	4.65
Mid-cingulate cortex	24/31	R	10	−20	42	5.34
		L	−4	−14	42	5.54
Posterior cingulate cortex	31	L	−12	−44	34	4.24
Inferior parietal lobule	40	R	50	−30	24	6.12
		L	−58	−26	20	6.34
Cuneus	19	R	14	−84	30	4.51
		L	−10	−84	28	4.43
Middle temporal gyrus	21	R	56	−22	−6	4.65
		L	−62	−24	−6	4.26
Superior temporal gyrus	22	R	50	8	−4	4.94
		L	−46	6	−4	5.45
Striatum (posterior putamen)		R	32	−10	2	4.95
		L	−28	−12	2	4.14
Amygdala/hippocampus		R	26	−6	−16	4.73
		L	−24	−10	−18	4.16

The reported regions were active with $Z > 3.1$ and a cluster size of at least 38 voxels. BA, Brodmann's area; R, right; L, left.

Table S2. Complete list of activations correlating negatively with the parametric |logLR| regressor used in the first main analysis of the fMRI data

Brain region	BA	Hemisphere	Peak MNI coordinates (mm)			*Z* value (peak)
			x	*y*	*z*	
Middle frontal gyrus	6	R	24	4	54	−5.22
		L	−26	−2	54	−4.34
	9/46	R	44	30	28	−4.86
		L	−44	26	26	−5.39
Inferior frontal gyrus	9	R	46	14	30	−4.93
		L	−42	10	32	−5.19
Anterior cingulate cortex (dorsal)	32	R	6	22	42	−6.18
		L	−6	18	44	−5.51
Insula (anterior)	13	R	34	24	−2	−5.60
		L	−32	24	−2	−5.81
Superior parietal lobule	39/40	R	32	−56	48	−5.32
		L	−38	−46	44	−4.58
Precuneus	7/19	R	34	−68	30	−4.91
		L	−28	−72	30	−4.63
Thalamus		R	10	−10	10	−4.61
		L	−8	−14	12	−4.86
Striatum (caudate)		R	10	12	4	−4.08
		L	−8	10	6	−4.42

The reported regions were active with $Z < -3.1$ and a cluster size of at least 38 voxels. BA, Brodmann's area; R, right; L, left.

Table S3. Activations in known reward-related regions showing a greater response to rewarded than unrewarded trials and vice versa during feedback

Brain region	BA	Hemisphere	Peak MNI coordinates (mm)			*Z* value (peak)
			x	*y*	*z*	
Rewarded > unrewarded						
Medial frontal gyrus	11	R	10	38	−10	6.45
		L	−2	−40	−12	6.14
Anterior cingulate cortex (ventral)	24/32	R	4	40	−4	6.11
		L	−4	48	−4	6.23
Striatum (ventral putamen)/nucleus accumbens		R	18	6	−10	4.82
		L	−16	6	−10	4.98
Striatum (posterior putamen)		R	34	−12	4	4.90
		L	−32	−12	2	5.16
Amygdala/hippocampus		R	24	−12	−18	6.09
		L	−24	−14	−18	5.87
Unrewarded > rewarded						
Insula (anterior)	13	R	40	22	−6	7.19
		L	−34	24	−4	6.76
Anterior cingulate cortex (dorsal)	6/32	R	6	26	40	5.92
		L	−2	22	42	4.66
Middle frontal gyrus	9/46	R	40	32	24	4.70
		L	−42	28	26	3.82
Striatum (caudate)		R	10	8	6	3.80
		L	−10	6	6	3.39

The reported regions were active with $Z > 3.1$ and a cluster size of at least 38 voxels. BA, Brodmann's area; R, right; L, left.